

DATA ACQUISITION AND AUTONOMOUS CONTROL OF FREE RUNNING SHIP MODELS USING VIDEO MOTION CAPTURE

Mathew Lamont¹
James Bowker^{1,2}
Nicholas Townsend^{1*}

¹Univeristy of Southampton, United Kingdom

²QinetiQ, Haslar Marine Technology Park

This paper presents the experimental setup and results from a new data acquisition and autonomous control system, using real time video motion capture feedback. The onboard data acquisition and control system, based on a National Instruments myRIO1900, was implemented in LabVIEW following a robotic architecture of sense-plan-act. A local wireless network was setup to view and control the real time LabVIEW VI from a laptop, with a Qualisys motion capture system used to track and stream (UDP) the model motions (6DOF) to the model in real time. The system, demonstrated on a 1:50 scale model bulk carrier model, was developed for comparative testing of an energy saving bow foil as part of the H2020 European SeaTech project (www.seatech2020.eu). The experimental setup and results from tests in the University of Southampton Boldrewood towing tank and the QinetiQ Haslar Ocean Basin are presented characterising the performance of the system. Results including propeller rpm control, rudder control (open and closed loop control), speed and heading control in calm water and in regular waves (streaming Qualisys motion data in real time) are presented. In addition, speed control under a moving carriage and autonomous waypoint following (including pure pursuit and line of sight methods) in the towing tank and Ocean Basin are presented. The results demonstrate the potential of the system for free running manoeuvring and seakeeping experiments. The presented data acquisition and control system software provides a new tool that can be applied in hydrodynamic ship model experiments, providing a flexible and modifiable framework for various hydrodynamic experimental investigations, reducing development time and costs associated with ship model testing.

1. Introduction

Currently, to comply with increasingly stringent regulations[1], national targets [2] and to reduce fuel consumption and greenhouse gas (GHG) emissions [3][4], experimental hydrodynamic ship efficiency and energy saving technologies is an active research area e.g., [5][6][7][8]. Within this research field, the use of free running models is gaining popularity [9][10][11][12], providing representative trajectory, kinematics and propulsion data (e.g., shaft torque and rpm) accurately and potentially at low cost compared to the alternatives e.g., constrained model experiments and computational modelling approaches. In the literature free running models have been developed for manoeuvring studies (e.g., straight line, circle and zig-zag manoeuvres [9][13][14]), propeller behaviour studies (e.g., constant rpm, power, torque tests [12]), adverse weather performance (e.g., wind and waves [15]), reproducing incidents (e.g., [16]) and autonomous guidance control studies (e.g., track-keeping [17], obstacle avoidance [18] and autonomous berthing [19]). Given the variety of experimental setups, investigations, and testing procedures e.g., fixed rpm versus fixed speed runs, developing flexible, reconfigurable data acquisition and control systems is a challenge.

This paper presents the experimental setup and results from a new LabVIEW data acquisition and control system. The system, which was developed for comparative testing of an energy saving bow foil as part of the H2020 European SeaTech project (www.seatech2020.eu), provides a flexible control system for a wide range of model scale, free running hydrodynamic and manoeuvring experiments. The system, based on a National Instruments myRIO1900, enables the performance of the model to be measured and displayed in real time under various and interchangeable control strategies (including manual, remote control, rpm, speed, rudder, heading and way-point following control). The approach uses a local wireless network to view and control the real time LabVIEW VI from a laptop (shore side) and a Qualisys motion capture system to track and stream (UDP) the model motions (6DOF) to the model in real time. The experimental setup, including the model hull design and the data acquisition and control system hardware and software is presented in Section 2. In Section 3 results from a series of experiments in the University of Southampton's Boldrewood towing tank and QinetiQ's ocean basin are presented, characterising and demonstrating the system propeller, rudder and waypoint following control options.

2. Experimental Setup

1.1. Model Hull Design

The ship model, Figure 1, is a generic small bulk carrier hullform. The model (and equivalent full scale) ship particulars are summarised in Table 1 and the linesplans are given in Figure 2. The dimensions were based on a collected ship database (of cargo carrying ships up to 10,000dwt) from freely available sources (primarily www.vesselfinder.com/vessels). The model equivalent full scale ship length (L_s) is nominally 100m (1:50 scale), although, as shown in Figure 3, the design remains representative for ship lengths between $L_s=50$ and 120 m (i.e., 1:25 and 1:60 scale). Based on the transverse stability of the nominal full scale ship and the International Code on Intact Stability [20], a mandatory stability criterion for cargo ships, the 'design' vertical centre of gravity (VCG) was set at 7m (0.14m) (from the keel) at full (model) scale.

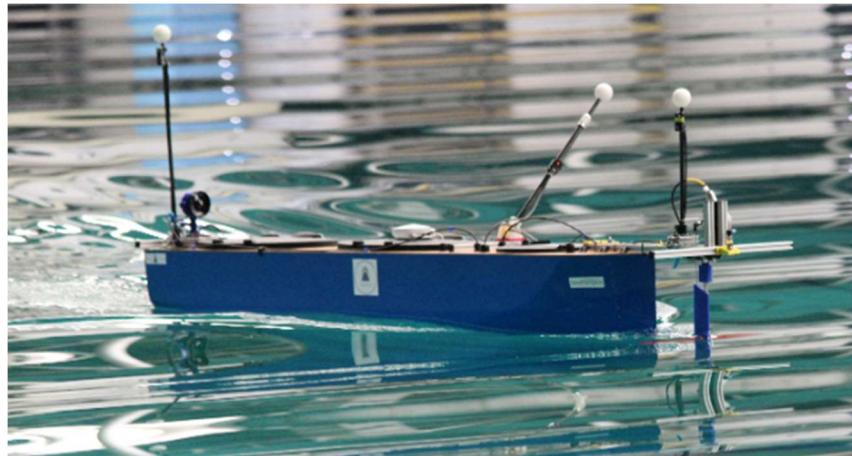


Fig. 1 – Ship model operating in waves [10]

Table 1 – Model and nominal full scale ship particulars

Hull Parameter	Model Scale	Nominal Full Scale
Vessel Type	Bulk Carrier	Bulk Carrier
Scale Ratio	1:50	1
Overall Length (L_{oa})[m]	2	100
Length between perpendiculars (L_{pp})[m]	2	100
Waterline Length (L_{wl})[m]	2	100
Breath (B)[m]	0.33	16.5
Draught (T)[m]	0.12	6
Freeboard [m]	0.17	8.65
Block Coefficient (C_b)	0.65	0.65
Prismatic Coefficient (C_p)	0.691	0.691
Length to Beam Ratio (L/B)	6.06	6.06
Beam to Draught Ratio (B/T)	2.75	2.75
Displacement [kg, Tonnes]	51.5	6600
Volumetric Displacement [m^3]	0.0515	6439
Water Plane Area [m^2]	0.545	1360
Wetted Surface Area [m^2]	0.836	2091
Trim [deg]	0	0
Longitudinal Centre of Gravity (LCG) [m]	0.005	0.25
Vertical Centre of Gravity (VCG) [m]	0.14	7
Longitudinal Metacentric Height (GM_l) [m]	2.627	130.8
Transverse Metacentric Height (GM_t) [m]	0.027	0.326
Longitudinal Centre of buoyancy (LCB)(+ fwd from midships)	0.005	0.25
Longitudinal Centre of floatation (LCF)(+ fwd from midships)	-0.067	-3.4
Roll Radius of gyration ($k_{44}=0.4B$)[m]	0.132	6.6
Pitch Radius of gyration ($k_{55}=0.25L_{pp}$)[m]	0.5	25
Yaw Radius of gyration ($k_{66}=0.25L_{pp}$)[m]	0.5	25

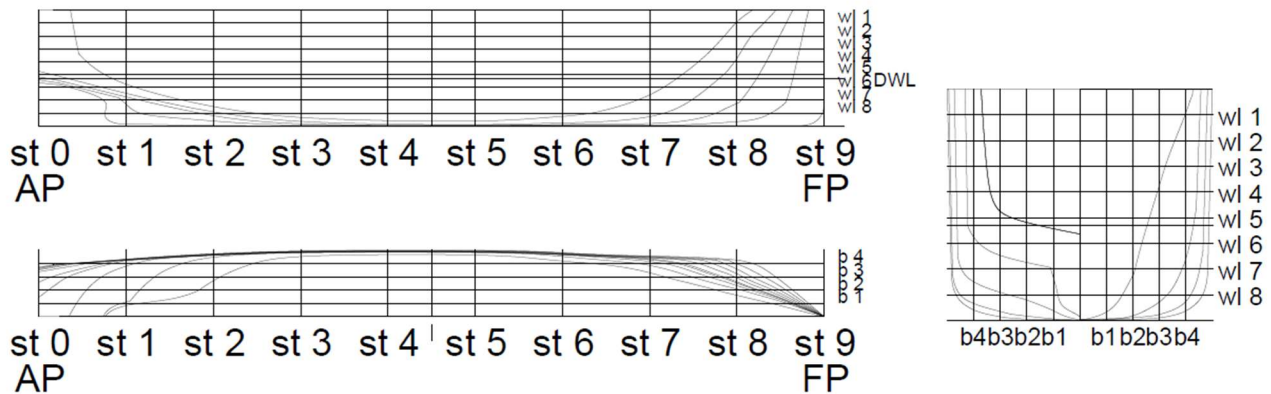


Fig. 2 – Hullform linesplan

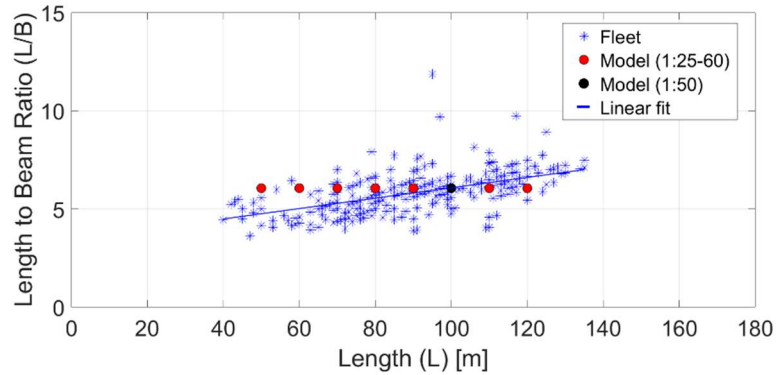


Fig. 3 – Comparison of length to beam ratio (L/B) of the design to collected database of cargo carrying ships up to 10,000 dwt (based on 478 ships, average ship length $\bar{L}=90.55\text{m}$, average ship beam $\bar{B}=15.63\text{m}$, average ship length to beam ratio $\bar{L}/\bar{B}=5.83$)

Skin Friction Correction Force: To account for the relatively greater contribution of skin friction at model scale (due to the difference in Reynolds number between model and full scale) and allow direct scaling of the measured delivered power to full scale, a skin friction correction (SFC) force is applied to the model. For a towed model, an offset can be applied to account for the skin friction correction (SFC) force [21], however, for a free running model this is not possible. To provide an additional thrust force, a ducted air fan was mounted to the stern via a load cell in order to calibrate and set the fan input control to the forward thrust. The setup, similar to that proposed in [11], is detailed in [10] and shown in Figure 4.

In addition, to promote similarity in the flow regime (such that the model scale is similar to the full scale turbulent flow) turbulence stimulation is widely applied to model ships. To provide turbulence stimulation the model is fitted with trip studs as detailed in Table 2 and shown in Figure 4.

Table 2 – Turbulence stimulation

Property	Value	Rationale
Stud height [mm]	2.5	Based on the Reynolds roughness criteria
Stud diameter [mm]	3.2	Based on similar models
Stud spacing [mm]	25	Following ITTC guidelines
Stud location [mm]	100	Typical position, 5% L

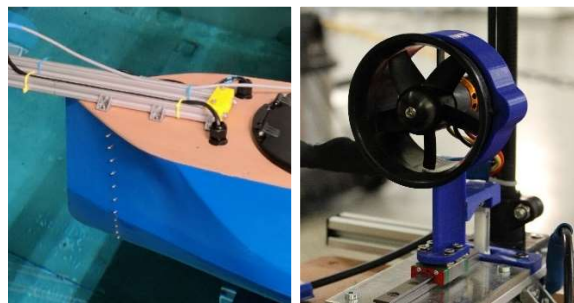


Fig. 4 – Photographs of the model showing (left) the trip studs and (right) the stern mounted ducted air fan for providing a skin friction correction force

Propulsion: A single screw propeller, driven by a DC motor in an in-line drive train arrangement, is used to propel the model, as shown in Figure 5. The stern tube was self-lubricating using external water and a 3D printed PLA drive train housing secured the drive train components to an aluminium base plate attached to the hull. A 75mm, 4 bladed brass propeller (Table 3 and 4) was selected. The target thrust of $\sim 2.5\text{N}$ was based on a calm water (Holtrop) resistance estimate (shown in Figure 6) (at the design speed 0.8m/s) with 50% sea margin, including a thrust deduction of 0.2, a SFC correction and a 20% margin for appendage drag, based on the Gawn propeller series [22] with the assumption that the hull efficiency $((1-\text{wake fraction})/(1-\text{thrust deduction}))$ is equal to 1, as summarised in Table 3. A 24V 30W brushless DC motor was selected based on the max speed power of 5.3W and a load capacity of 300% (assuming a conservative shaft efficiency of 0.5).

Table 3 – Propeller design (^aHoltrop, 0.8m/s) (^b50% sea margin) (^cbased on gawn propeller series)

Parameter	Calm	Seaway	Max speed
Resistance [N]	1.7 ^a	2.5 ^b	n/a
Shaft Rotation [RPM]	925	1100	1250
Density, ρ [kg/m^3]	1000	1000	1000
Model Speed, V [m/s]	0.8	0.8	1
J	0.692	0.582	0.64
K_t ^c	0.211	0.257	0.234
K_q ^c	0.036	0.042	0.039
Eta ^c	0.645	0.583	0.616
Thrust [N]	1.587	2.737	3.218
Torque [Nm]	0.02	0.034	0.04
Power [W]	1.967	3.877	5.299

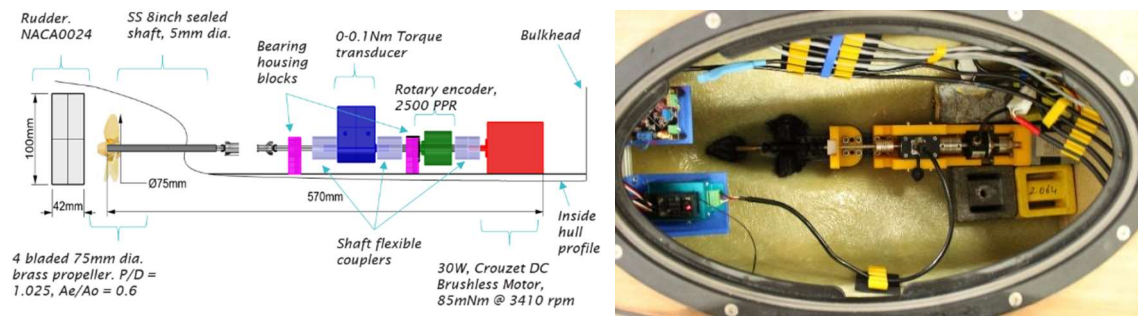


Fig. 5 – Schematic and photograph of the drivetrain in the aft compartment

Table 4 – Model propeller properties

Property	Value	Comment / Rationale
Propeller blades	4	Raboesch R/H Brass A-Type Propeller
Propeller diameter [mm]	75	
Propeller P/D ratio	1.025	
Propeller A_e/A_o ratio	0.6	
Propeller tip clearance [mm]	20.25	Typ. $\leq 25\%D$
Propeller rudder spacing [mm]	24	Typ. 0.3 to 0.35D
Crouzet Brushless DC Motor [W]	35	24V Brushless DC motor with 6mm shaft diameter

Steering: A single, fully balanced rudder is used to steer the model, as shown in Figure 6. The rudder area was geometrical scaled following guidelines based on the ship lateral area [23], and for simplicity a NACA0024 profile section was selected providing reasonable thickness for a rudder stock at 25%C (measured from the leading edge). The rudder design is detailed in Table 6. The rudder was 3D printed in PLA (100% infill) with a 5mm diameter stainless steel rudder shaft. The hull, rudder and propeller clearances followed the recommendations in [24].



Fig. 6 – General arrangement and photo of the rudder and propeller clearance

Table 5 – Model rudder properties

Property	Value	Comment / Rationale
Rudder area [mm ²]	4200	Typ. Area / (L×T) ≥ 1.7
Rudder span [mm]	100	2.5mm from keel
Rudder chord [mm]	42	Aligned with transom
Rudder stock	25%	of the chord length
Rudder section	NACA0024	Fully balanced rudder
Rudder material	PLA	3D printed, 100% infill

1.2. Data Acquisition and Control

Hardware: The on-board data acquisition and control system is based on a National Instruments myRIO-1900 and LabVIEW software. A local wireless network is setup to view and control the real time LabVIEW VI (running on the myRIO, located in the central watertight compartment of the model) from a remote laptop, as shown in Figure 7. The real time VI acquires data from the installed sensors (Table 6) and saves the data to the USB flash drive. Although, the setup described uses a commercial Qualisys video motion capture to UDP stream the 6DOF model motions directly to the myRIO, this could be replaced using a number of alternatives e.g., GNSS, dead reckoning estimation etc. The model is powered from a Vruzend DIY solderless lithium-Ion battery pack (24V), comprised of SAMSUNG 25R 18650 2500mAh cells arranged in an 7s7p configuration.

Table 6 – Installed sensors (including the bow foil sensor setup)

Sensor	Type	Range	Additional information
Shaft torque meter	Full bridge	0-0.1 Nm	Miniature dynamic torque sensor (0-0.1N.m)
Shaft encoder	Optical	2500ppr	CALT rotary incremental hollow shaft encoder
SFC Load cell	Full bridge	±5N	Straight bar mini load cell (500g)
Rudder potentiometer	Resistance	±50deg	RS PRO 10kΩ rotary wire-wound potentiometer
Accelerometer	Tri-axial	± 8g	myRIO-1900, 3 axis accelerometer
Wave probe	Ultrasonic	30-500mm	RS PRO Ultrasonic Proximity Sensor (IP67)

Tri-axial load cell	Half bridge	$\pm 10\text{N}$	Forsentek 3 axis load cell (10N)
Foil pitch encoder	Optical	2048ppr	Baumer incremental digital encoder
Video motion capture	Optical	-	Qualisys video motion capture system
Facility wave probes	Ultrasonic	0.05-2.5m	

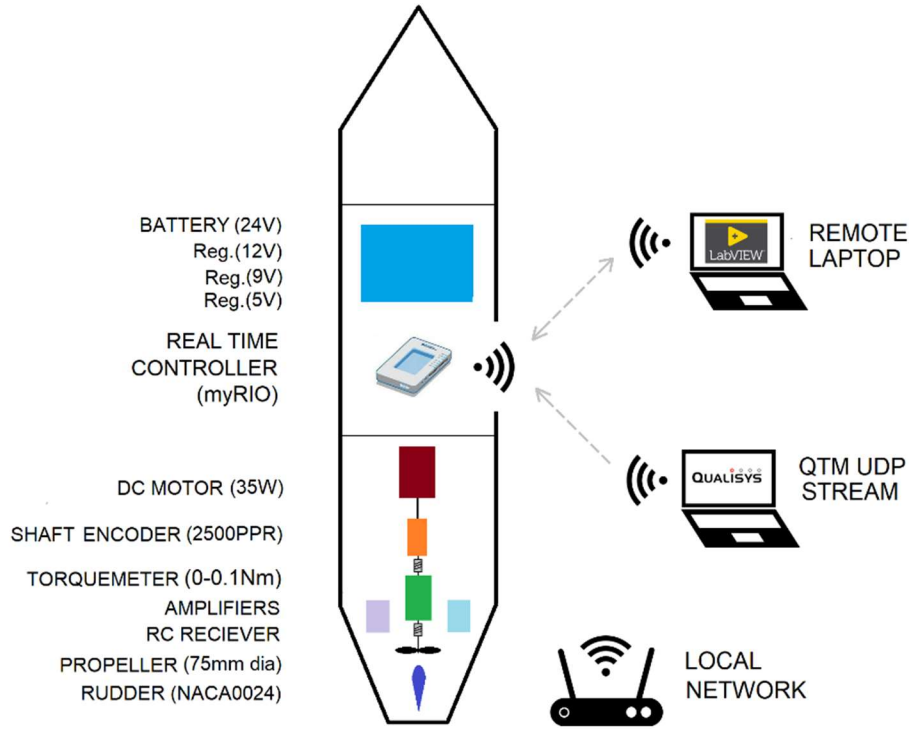


Fig. 7 – Experimental Setup

Software: The model data acquisition and control software is coded in LabVIEW and directly run on the NI myRIO-1900. The LabVIEW Virtual Instruments (VI) architecture is summarised in Figure 8. The code provides multiple control options for the SFC fan, propeller and rudder servo, and can be readily modified allowing for the study of various energy saving devices (ESDs) and/or on-board systems. As summarised in Tables 7 and 8, PWM control signals generated by the myRIO-1900, are used to control the SFC fan via an electronic speed controller (ESC), the propeller motor and the rudder servo.

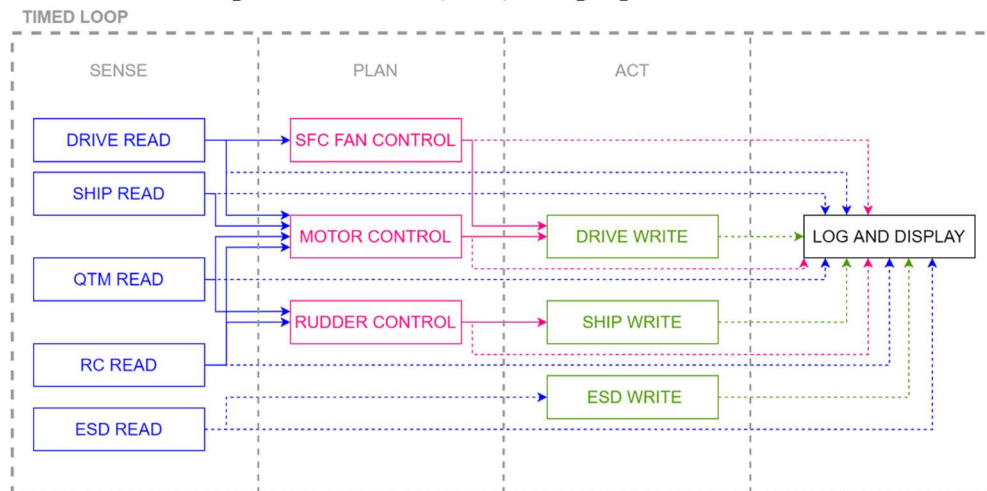


Fig. 8 – Overview of LabVIEW VI Architecture

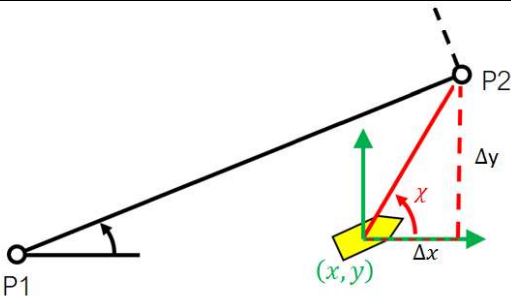
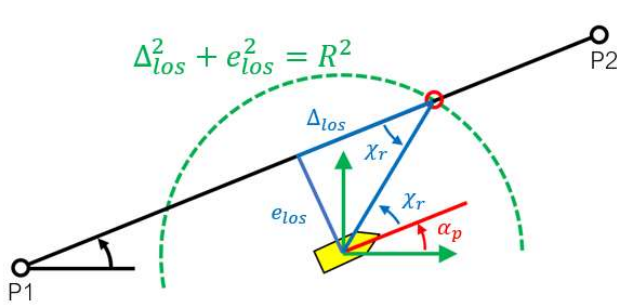
Table 7 – Propeller control options

Control	Method	Description
Remote Control (RC)		Motor command based on remote control (handset) input
Manual Control (%)		Motor command based on manual percentage input (on main VI)
RPM (PID)		PID control of shaft rpm based on shaft encoder reading, rpm setpoint on main VI
Forward Speed (PID)		PID control of model forward speed (U) based on QTM streamed data

Table 8 – Rudder control options (the waypoint guidance options are summarised in Table 11)

Control	Method	Description
Manual Control (%)		Rudder command based on manual percentage input (on main VI)
Remote Control (RC)		Rudder command based on remote control (handset) input
Rudder Control (open and closed loop)	<p>Open Loop</p>	Open loop control: command based on rudder angle setpoint on main VI
	<p>Closed Loop</p>	Closed loop control: PID control of rudder angle based on rudder potentiometer reading, rudder angle setpoint on main VI
Heading Control (PID)		PID control of model heading (χ) based on QTM streamed (yaw) data, heading angle setpoint on main VI.
Waypoint Control (PID)		PID control of heading angle based on assigned guidance heading angle, calculated using QTM streamed data. Options for pure pursuit and line of sight guidance (see Table 9)

Table 9 – Waypoint guidance control options

Control	Method	Description
Pure pursuit (PP)		<p>2-point guidance, direct assignment of heading to next waypoint</p> $\chi = \text{atan2}(y_{wp} - y, x_{wp} - x)$ <p>Waypoint switching based on radius of acceptance</p>
Line of Sight (LOS)		<p>3-point guidance, heading comprised of the tangential path angle plus the relative line of sight heading angle</p> $\chi = \alpha_p + \tan^{-1}\left(-\frac{e_{los}}{\Delta_{los}}\right)$ <p>Waypoint switching based on radius of acceptance</p>

3. Results

1.1. Propeller Control

Figure 9 demonstrates the feedback control of the shaft rotation.

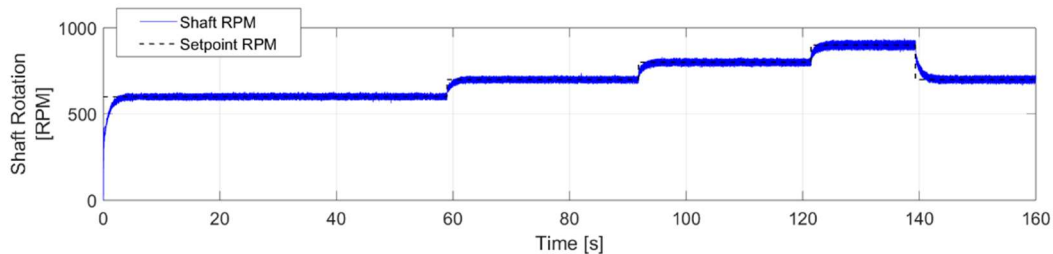


Fig. 9 – Shaft rotation step responses (Stepping between 600rpm, 700rpm, 800rpm and 900rpm)
($K_c=0.01$, $T_i(\text{min})=0.005$)

Figure 10 shows the speed control of the model in calm water. Starting from rest, the presented runs which comprised of turning the SFC fan on followed by directly enabling speed control, demonstrate the repeatably of the control system. Due to motion tracking and streaming data dropouts (Figure 10(a)), a low pass (0.1Hz) filter was applied (Figure 10(b)). The shaft rpm ramped up and settled once the model achieved the design speed (0.8m/s) (Figure 10(b)).

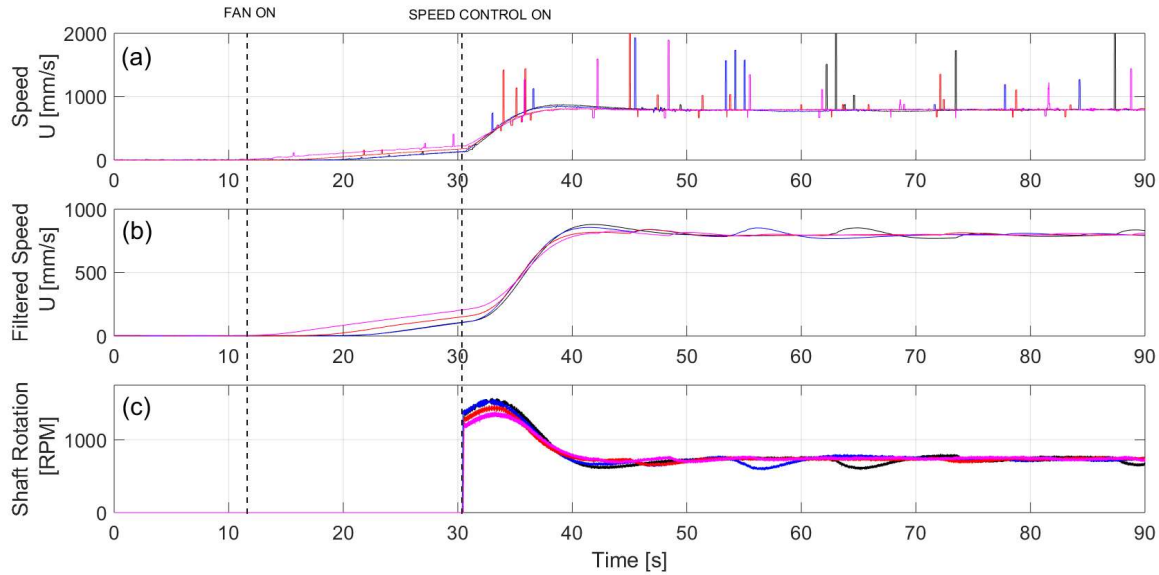


Fig. 10 – Speed control of the model in calm water ((a) Model speed (mm/s) (b) 0.1Hz low pass filtered speed (mm/s) (c) Shaft rotation (rpm)) (Note: Runs presented include both 0° (black, blue) and 30° (red, magenta) heading demonstrating the model speed control over a range of headings) ($Kc=40, Ti(min)=0.15$)

Figure 11 shows the speed control of the model in waves. Initially the model accelerates to the design speed in calm water (Figure 11(a)), then encounters waves (Figure 11(c)). Here, as expected, due to the added resistance in waves the controller leads to an increase in rpm to maintain the set design speed (Figure 11(b)).

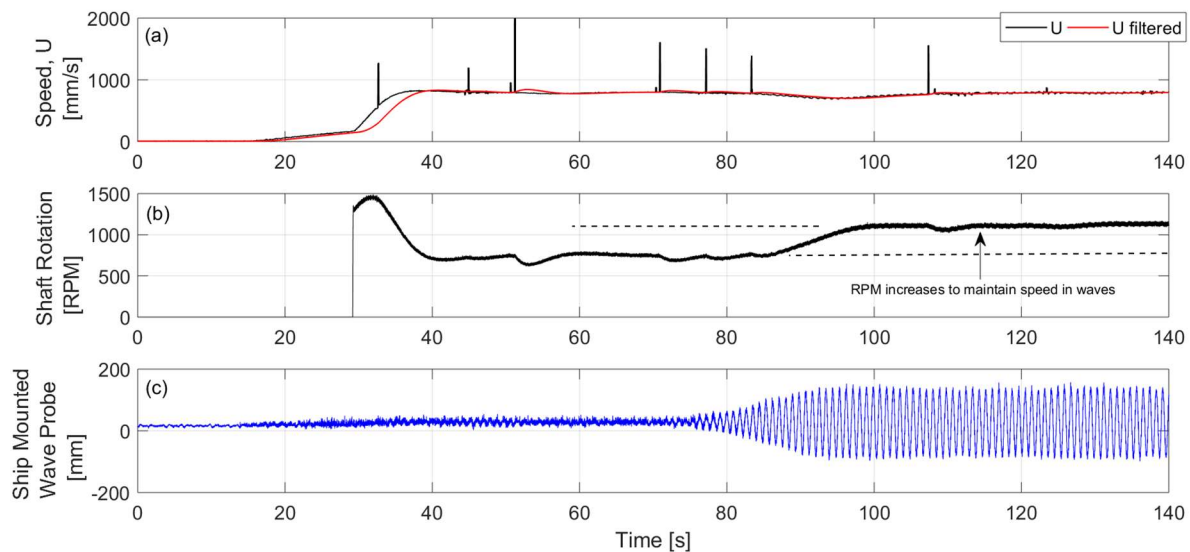


Fig. 11 – Speed control of the model encountering regular waves ((a) Filtered and unfiltered model speed (mm/s) (b) Shaft rotation (rpm) (c) Relative wave probe signal (mm)) (0° Heading, $f= 0.8\text{Hz}$, $\zeta_0=0.02\text{m}$) ($Kc=40, Ti(min)=0.15$)

In addition, by setting the target velocity to zero, the control system was tested to ascertain if the model would track the speed of a moving carriage (and the attached Qualisys reference) in the towing tank. The results presented in Figure 12, shows the measured relative speed (from the carriage moving at 0.8m/s) and shaft rpm from runs (of increasing wave height) initially in calm water then encountering regular waves. The results show that as the model encounters the waves, the rpm increases to maintain speed, and the control system can be used to track the carriage, in calm water and in waves.

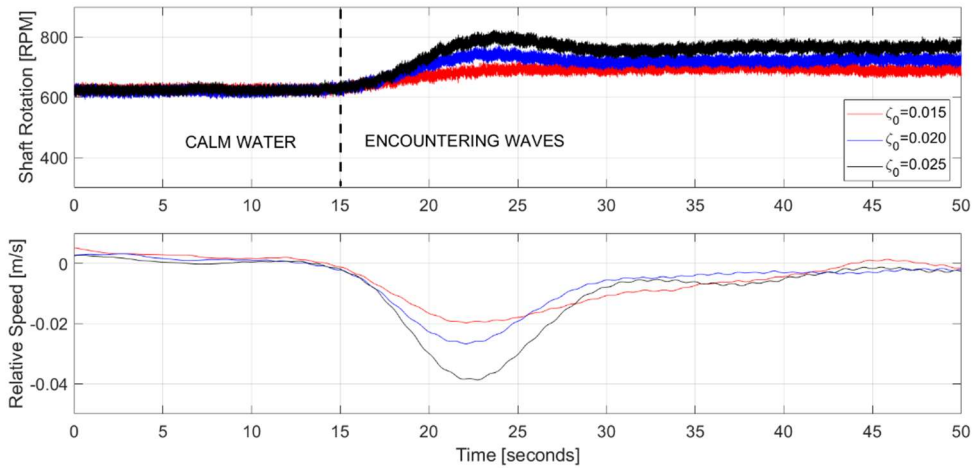


Fig. 12 – Propeller rpm and carriage speed tracking of the model encountering regular waves ($f=0.7\text{Hz}$, $\zeta_0=0.015,0.020,0.025\text{m}$) (0.1Hz low pass filtered relative speed presented)

1.2. Rudder Control

Figure 13 shows the open loop and closed loop control of the rudder. These examples, which show a series of step responses ($\pm 20^\circ$), demonstrates the repeatability of the rudder angle control.

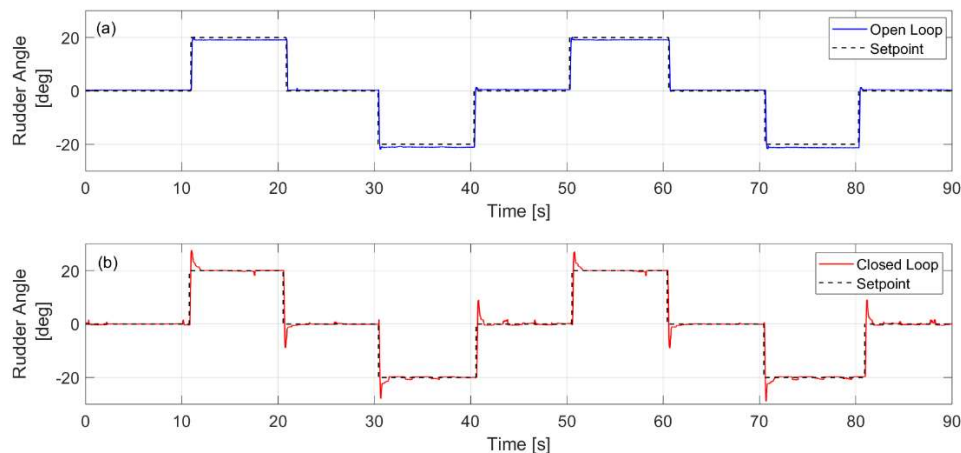


Fig. 13 – Rudder angle control ((a) Open loop control (b) Closed loop (feedback) control using the rudder potentiometer ($K_c=1.0$, $T_i(\text{min})=0.006$)

Figure 14(a) shows the response to a 90° change in heading command of the model under fixed rpm control in calm water. In this example, the measured rudder angle (Figure 14(b)) initially goes hard over, before returning to a neutral position once the heading angle is achieved.

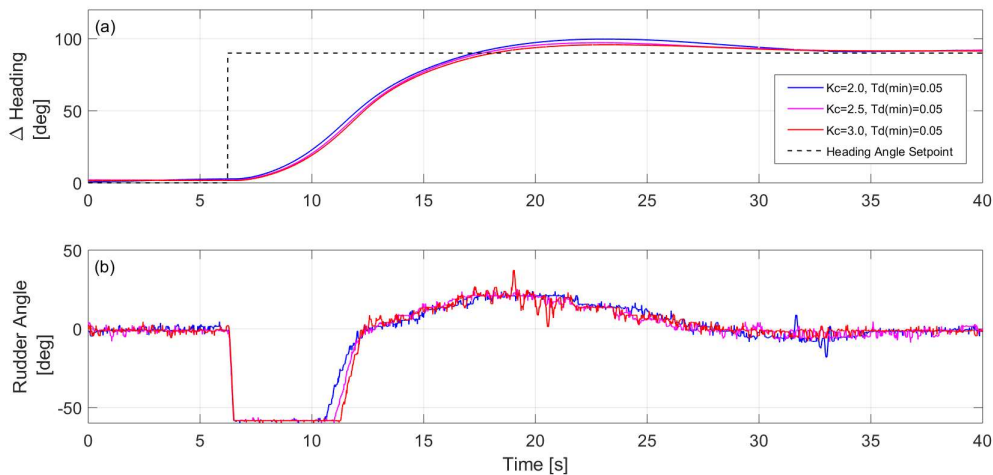


Fig. 14 – Heading control and rudder response to a 90° change in heading command in calm water ((a) Heading angle ($^\circ$) (b) Rudder angle ($^\circ$) (Fixed 700rpm)

Figure 15 shows heading control (0° , 30° , 60° and -90°) of the model when operating in regular waves (0.7, 0.8 and 0.9Hz). The control successfully maintained the heading under wave disturbances.

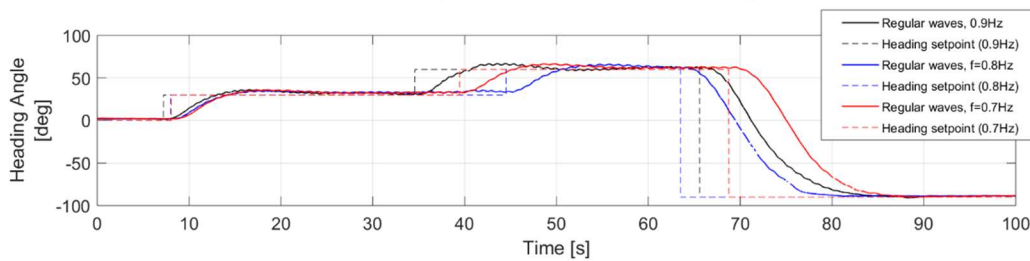


Fig. 15 – Heading control in regular waves ($0.8m/s$, $\zeta_0 = 0.02m$, $Kc = 3.0$, $Td(min) = 0.05$)

Figure 16 illustrates the performance difference between an experienced remote-control operator and the feedback heading control, operating in regular waves. For an experienced RC operator, visually maintaining the heading, the measured heading standard deviation was ~ 0.9 , compared to ~ 0.15 under feedback control.

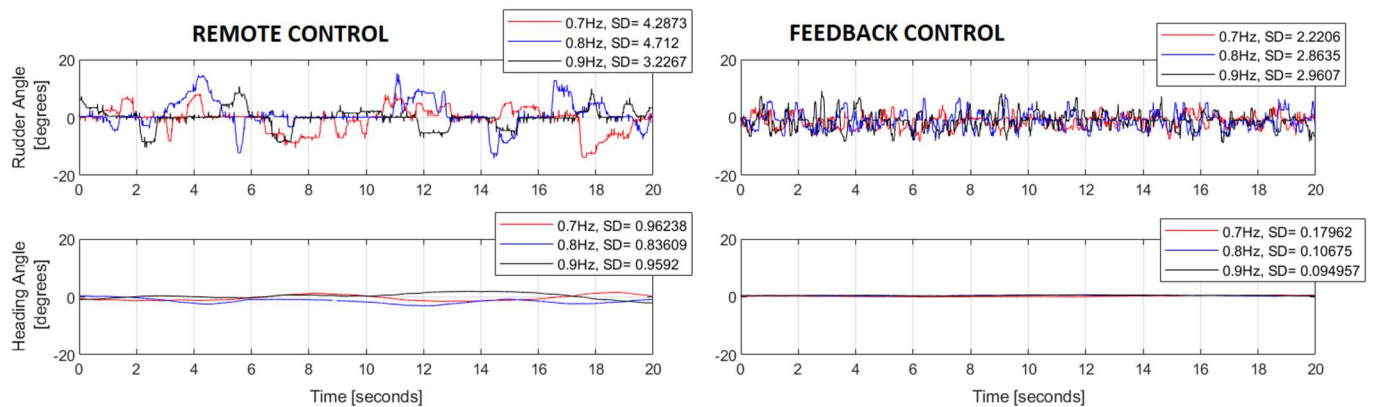


Fig. 16 – Comparison of remote control and feedback heading control in regular waves (Top: rudder angle in degrees, bottom: heading angle in degrees) ($\chi = 0^\circ$, $f=0.7,0.8,0.9Hz$, $\zeta_0=0.02m$, $U=0.8m/s$)

1.3. Waypoint Guidance Control

Figure 17 demonstrates the way-point following under pure pursuit (PP) and line of sight guidance (LOS) methods. The way-points were selected to represent a lawn mower pattern with port and starboard turns. Figure 18 show the line of sight guidance of the model in calm water then in regular waves.

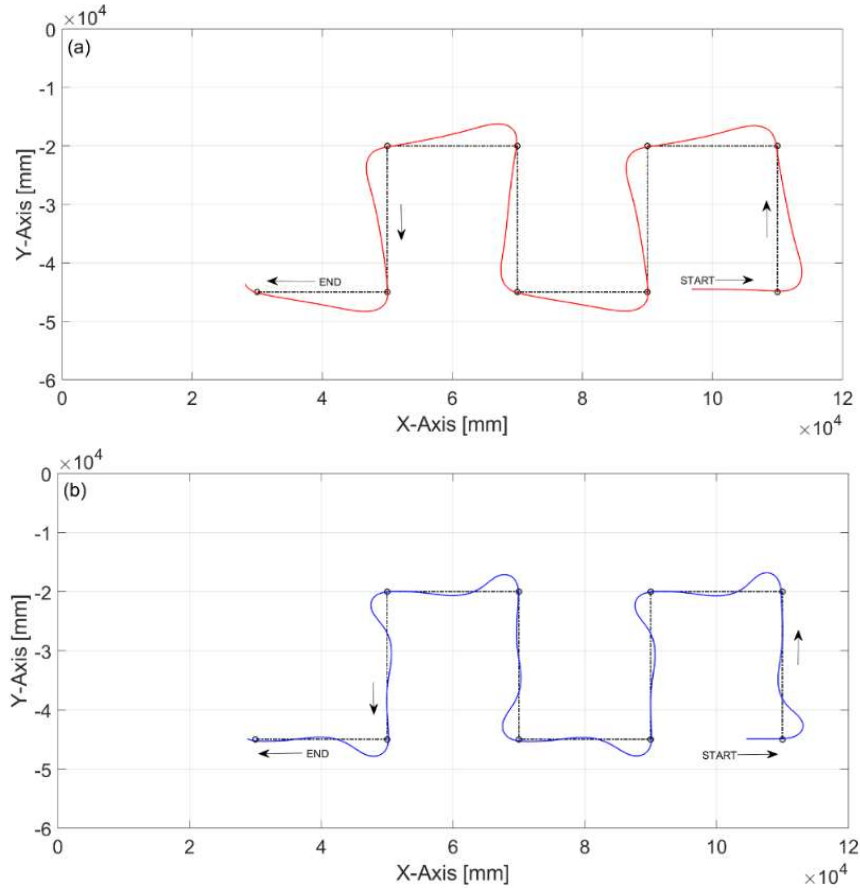


Fig. 17 – Way-point following in calm water ((a) Pure pursuit guidance (b) Line of sight (enclosure based, $R_{los} = 4m$) guidance) (Acceptance radius 2m) (Fixed 800rpm)

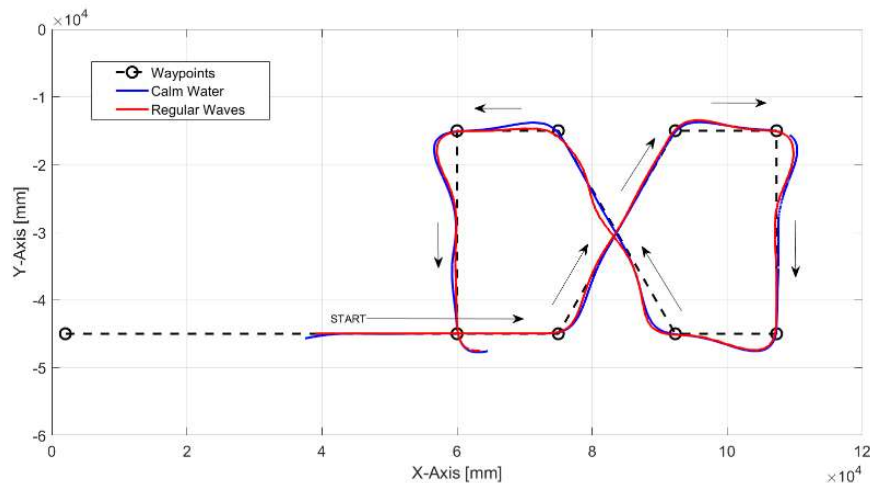


Fig. 18 – Line of Sight way-point following in calm water and regular waves ($f=0.8Hz$, $\zeta_0=0.025m$, $U=0.8m/s$)

4. Discussion

This paper presents the experimental setup and results from a new LabVIEW based data acquisition and autonomous control system, using real time video motion capture (Qualisys) feedback for ship model testing. The results, collected over a period of time from a series of tests in the University of Southampton towing tank (Length = 138 m, Breadth = 6 m, Depth = 3.5 m) and the QinetiQ ocean basin (Length = 120 m, Breadth = 60 m, Depth = 5 m), demonstrates the flexibility and repeatability of the system and results. As exemplified by remote controlled operation and feedback heading control comparison (Figure 17), the accuracy and precision of the results can be improved through the use of autonomous and feedback control approaches. Although, the setup described uses a commercial Qualisys video motion capture to UDP stream the 6DOF model motions directly to the myRIO, this could be replaced, for example with GNSS or dead reckoning estimation, to enable lake or coastal tests to be conducted in the future. For assessing ship energy efficiency, the system has been used to assess the performance of ship bow foils (see [10], [25]), in particular enabling a direct comparison of the response with and without an energy saving bow foil encountering the same irregular waves, through the controlled release and autonomous speed control to a repeated seeded wave spectrum [26].

5. Conclusions

This paper presents the experimental setup and results from a new LabVIEW based data acquisition and autonomous control system, using real time video motion capture (Qualisys) feedback, for free-running ship model experiments. The design and experimental results demonstrate and characterise the performance of the system, highlighting the potential of the system for a range of experimental studies. The system is hoped to reduce development time and costs associated with ship model testing.

6. References

- [1] IMO, “Guidelines on the method of calculation of the attained energy efficiency existing ship index (EEXI) (resolution MEPC.350(78)),” 2022.
- [2] “Maritime 2050 Navigating the future ,” 2019.
- [3] E. A. Bouman, E. Lindstad, A. I. Riialand, and A. H. Strømman, “State-of-the-art technologies, measures, and potential for reducing GHG emissions from shipping—A review,” *Transp Res D Transp Environ*, vol. 52, pp. 408–421, 2017.
- [4] T.-H. Joung, S.-G. Kang, J.-K. Lee, and J. Ahn, “The IMO initial strategy for reducing Greenhouse Gas (GHG) emissions, and its follow-up actions towards 2050,” *Journal of International Maritime Safety, Environmental Affairs, and Shipping*, vol. 4, no. 1, pp. 1–7, 2020.
- [5] K. Belibassakis, S. Bleuanus, J. Vermeiden, and N. Townsend, “Combined performance of innovative biomimetic ship propulsion system in waves with Dual Fuel ship engine and application to short-sea shipping,” in *ISOPE International Ocean and Polar Engineering Conference*, ISOPE, 2021, p. ISOPE-I.
- [6] Z. Guangrong, “Ship energy efficiency technologies: Now and the future,” 2017.
- [7] ITTC, “International towing tank conference,” in *Specialist Committee on Energy Saving Method*, 2021.
- [8] ABS, “ABS advisory on ship energy efficiency measures.”

- [9] A. M. Bassam, A. B. Phillips, S. R. Turnock, and P. A. Wilson, "Experimental testing and simulations of an autonomous, self-propulsion and self-measuring tanker ship model," *Ocean Engineering*, vol. 186, p. 106065, 2019.
- [10] J. A. Bowker and N. C. Townsend, "Evaluation of bow foils on ship delivered power in waves using model tests," *Applied Ocean Research*, vol. 123, p. 103148, 2022.
- [11] M. Ueno and Y. Tsukada, "Estimation of full-scale propeller torque and thrust using free-running model ship in waves," *Ocean Engineering*, vol. 120, pp. 30–39, 2016.
- [12] A. Coraddu, G. Dubbioso, S. Mauro, and M. Viviani, "Analysis of twin screw ships' asymmetric propeller behaviour by means of free running model tests," *Ocean Engineering*, vol. 68, pp. 47–64, 2013.
- [13] G. Dubbioso, S. Mauro, and M. Viviani, "Off-design propulsion power plant investigations by means of free running manoeuvring ship model test and simulation techniques," in *ISOPE International Ocean and Polar Engineering Conference*, ISOPE, 2011, p. ISOPE-I.
- [14] J. Zheng, F. Meng, and Y. Li, "Design and experimental testing of a free-running ship motion control platform," *IEEE Access*, vol. 6, pp. 4690–4696, 2017.
- [15] R. Suzuki, Y. Tsukada, and M. Ueno, "Estimation of full-scale ship manoeuvrability in adverse weather using free-running model test," *Ocean Engineering*, vol. 213, p. 107562, 2020.
- [16] M. Ueno, H. Miyazaki, H. Taguchi, Y. Kitagawa, and Y. Tsukada, "Model experiment reproducing an incident of fast ferry," *J Mar Sci Technol*, vol. 18, pp. 192–202, 2013.
- [17] N. Im, V.-L. Tran, and T.-D. Le, "Experiment on track-keeping performance using free running model ship," *IFAC Proceedings Volumes*, vol. 46, no. 33, pp. 126–131, 2013.
- [18] D. F. Carlson *et al.*, "An affordable and portable autonomous surface vehicle with obstacle avoidance for coastal ocean monitoring," *HardwareX*, vol. 5, p. e00059, 2019.
- [19] Y. A. Ahmed and K. Hasegawa, "Implementation of automatic ship berthing using artificial neural network for free running experiment," *IFAC Proceedings Volumes*, vol. 46, no. 33, pp. 25–30, 2013.
- [20] IMO, "International Code on Intact Stability," 2018.
- [21] J.-H. Seo, C.-M. Lee, J.-W. Yu, J.-E. Choi, and I. Lee, "Power increase and propulsive characteristics in regular head waves of KVLCC2 using model tests," *Ocean Engineering*, vol. 216, p. 108058, 2020.
- [22] R. W. L. Gawn, "Effect of pitch and blade width on propeller performance," in *Autumn Meeting of the Institution of Naval Architects, TINA, Rome, Italy, 1953, pp. 157-193, RINA Transactions 1953-09*, 1953.
- [23] J. Liu and R. Hekkenberg, "Sixty years of research on ship rudders: effects of design choices on rudder performance," *Ships and offshore structures*, vol. 12, no. 4, pp. 495–512, 2017.
- [24] A. F. Molland, S. R. Turnock, and D. A. Hudson, *Ship resistance and propulsion*. Cambridge university press, 2017.
- [25] J. A. Bowker and N. C. Townsend, "A probabilistic method to evaluate bow foils for realistic seas and shipping routes," *Applied Ocean Research*, vol. 129, p. 103374, 2022.
- [26] J. Bowker, N. Townsend, N. Bulten, and S. Bleuanus, "Comparison of ship energy efficiency methods for bow foil technology," in *OCEANS 2023-Limerick*, 2023.